

A theoretical study of the role of astrocyte activity in neuronal hyperexcitability using a new neuro-glial mass model

Aurélie Garnier ^{*‡}, Alexandre Vidal [†], Habib Benali ^{*}

March 3, 2022

Abstract

The investigation of the neuronal environment allows us to better understand the activity of a cerebral region as a whole. The recent experimental evidences of the presence of transporters for glutamate and GABA in both neuronal and astrocyte compartments raise the question of the functional importance of the astrocytes in the regulation of the neuronal activity. We propose a new computational model at the mesoscopic scale embedding the recent knowledge on the physiology of neuron and astrocyte coupled activities. The neural compartment is a neural mass model with double excitatory feedback, and the glial compartment focus on the dynamics of glutamate and GABA concentrations. Using the proposed model, we first study the impact of a deficiency in the reuptake of GABA by astrocytes, which implies an increase in GABA concentration in the extracellular space. A decrease in the frequency of neural activity is observed and explained from the dynamics analysis. Second, we investigate the neuronal response to a deficiency in the reuptake of Glutamate by the astrocytes. In this case, we identify three behaviors : the neural activity may either be reduced, or enhanced or, alternatively, may experience a transient of high activity before stabilizing around a new activity regime with a frequency close to the nominal one. After translating theoretically the neuronal excitability modulation using the bifurcation structure of the neural mass model, we state the conditions on the glial feedback parameters corresponding to each behavior.

Keywords: Model in Neuroscience, Qualitative analysis of dynamical systems, Bifurcations, Neuro-glial interactions, GABAergic and glutamatergic neurotransmissions, Excitability modulation, Neuronal hyperexcitability

AMS classification: 34C15, 34C23, 34C28, 34C46, 34C60, 34H20, 92C20, 92B25.

1 Introduction

For several years, to understand the mechanisms of the cerebral metabolism has become an important issue in neuroscience. The investigation of the neural environment allows us to better understand the activity of a cerebral region as a whole. For instance, the neural activity is composed of an interplay between excitation and inhibition where the cerebral blood flow (CBF) dynamics is an essential element as it reflects nutrients supplies such as oxygen and glucose. Synaptic transmission [1, 2, 15, 25, 39] and neural activity [13, 16, 27] are regulated by neurotransmitters, ions and molecules. Broadly speaking, at the microscopic scale, the presynaptic neuron releases neurotransmitters in the synaptic cleft which may bind to postsynaptic neuron receptors. These receptors, when “activated” by neurotransmitters, trigger ions exchanges between the extracellular space and the postsynaptic neuron that can induce the activation of the postsynaptic neuron. Parallely, neurotransmitter in the extracellular space may bind to astrocytic receptors and transporters inducing the activation of the glial calcic cycle allowing to release glutamate in the extra-synaptic space.

The demonstration of the presence of transporters for glutamate and GABA in both neural and astrocyte compartments raises the question of the functional importance of the astrocytes in the regulation of the neural activity [38]. It has been shown that glial cells and particularly astrocytes have a great impact on both the metabolic regulation [31] and the CBF dynamics [20]. Indeed, astrocytes modulate the dynamics of neurotransmitter concentrations, and thus the neuronal excitability, the synaptic transmission and the neural activity. Consequently, astrocytes dysfunctions are involved in several brain pathologies [21, 28, 32]. Studying the interactions between the neurons and astrocytes cells has therefore become an essential problem in neurophysiology and biophysics.

^{*}Sorbonne Universités, UPMC Univ Paris 06, CNRS, INSERM, Laboratoire d’Imagerie Biomédicale (LIB), F-75013 Paris, France

[†]Laboratoire de Mathématiques et Modélisation d’Évry (LaMME), CNRS UMR 8071, Université d’Évry-Val-d’Essonne, F-91000 Évry, France

[‡]aurelie.garnier@lib.upmc.fr

In this context, computational models provide a key tool for interpreting the observed electrophysiological data and for revealing the different (patho-)physiological mechanisms which may underlie the observational data. Several models including the metabolic regulation mechanisms have been proposed in the literature. Some authors have built models of tripartite synapse [24, 29, 30, 36, 37] considering an astrocyte coupled with a presynaptic neuron and a postsynaptic one and the dynamics of neurotransmitters, ions and molecules. Other authors considered a single neuron coupled with an astrocyte [10, 14, 33, 36] and sometimes with a hemodynamic compartment [3, 4, 5] and the dynamics of neurotransmitters, ions and molecules between and in these elements. Recently, a new mesoscopic computational model [7] focusing on the astrocyte dynamics has been proposed. This model links the neural activity measured by local field potentials (LFP) to the CBF dynamics measured by Laser Doppler (LD) recordings through glial activity. The model incorporates the astrocyte cells via their role in neurotransmitters (glutamate and GABA) recycling, with physiologically-relevant relationships between these variables.

In this article, we propose a model extending the one presented in [7] for studying the neuro-glial interactions and more particularly the impact that the astrocyte activity may have upon the neuronal one. We use the same organization embedding a neural compartment and a glial one. To reproduce the mesoscopic neural activity, we use the neural mass model (NMM) with double excitatory feedback presented in [12] which generalizes the Jansen-Rit model used in [7]. We keep the glutamate and GABA dynamics presented in [7] for the glial compartment. In this model, the neural activity acts on glutamate and GABA dynamics through the pyramidal and interneuronal firing rates respectively. The essential extension in our model consists in embedding the influence of the glial dynamics upon neural activity through the glutamate and GABA extracellular concentrations. Indeed, physiologically, a pyramidal cell (resp. an interneuron) releases glutamate (resp. GABA) in the synaptic cleft from where it binds to receptors on the postsynaptic neuron and the astrocyte. Reuptake processes (referred to as “reuptakes” in this article) of the neurotransmitters by the local astrocyte and presynaptic neuron regulates their concentration in the extracellular space (Figure 1). In the presynaptic neuron, the reuptake completes the stock whereas the reuptake by the astrocyte triggers a cascade of reactions linked with the modulation of synaptic transmission (differentially according to the type of neurotransmitters) and the hemodynamics. Hence, we introduce a feedback coupling from the glial compartment upon the neural one in our model. This feedback, referred to as the “glial feedback” in this article, allows us to study how different astrocyte deficiencies impact the local neuro-glial activities. If the mechanism of glutamate or GABA reuptake by the astrocytes is deficient, the neurotransmitter accumulates in the synaptic cleft, which leads to an increase in its concentration in the extracellular space. When this concentration reaches a threshold the synaptic transmission to postsynaptic neuron becomes abnormal and the postsynaptic neuron excitability threshold changes.

The proposed model provides a unified framework in which knowledge of the physiology of neuron and astrocyte activities, as well as their couplings, can be incorporated, in order (i) to simulate the output signals for chosen parameter values, (ii) to identify the various qualitative responses of the whole system to physiological disorders, (iii) to study theoretically the conditions over the parameters corresponding to each type of response. The neural mass approach offers therefore an optimal compromise between the compactness of the dynamics, the richness of the physio-pathological mechanisms that can be reproduced, and the interpretability of the parameters from the biophysical viewpoint. The range of parameter values can be inspired from physiology-based studies in actual animal models. Once the parameter range is defined, one can test the influence of varying a reduced set of parameters (for example, ratio between excitation and inhibition or Glutamate and GABA reuptake) on the output signals.

The paper is organized as follows. In section 2, we discuss the main pathways of the neuro-glial interactions. We recall the dynamical features that explain the qualitative and quantitative properties of the time series generated by each compartment. In particular, we describe the bifurcation structure of the neural compartment underlying the generation of Noise Induced Spiking (NIS) outputs on which we focus in this article [12]. We introduce the bilaterally coupled model and illustrate the main difference with the feedforward model by mimicking the injection of a GABA bolus in the extracellular space. In section 3, we study theoretically the effect of a deficiency of the GABA reuptake by the astrocyte upon the neural system behavior, we illustrate the result by numerical simulations and link the observed outputs with known biological results. In section 4, we identify and illustrate numerically the three possible responses of the neural compartment to a deficiency of the glutamate reuptake by the astrocyte : reduced activity, transient and permanent hyperexcitability. We explain this spectrum of responses using the analysis of the dynamical structure of the model and we derive explicit conditions on the parameters involved in the glial feedback corresponding to each type of behaviors. Finally we interpret the conditions on the parameters in terms of physio-pathological features and discuss possible applications of this study for investigating experimentally the precise role of astrocyte deficiencies in neuronal hyperexcitability.

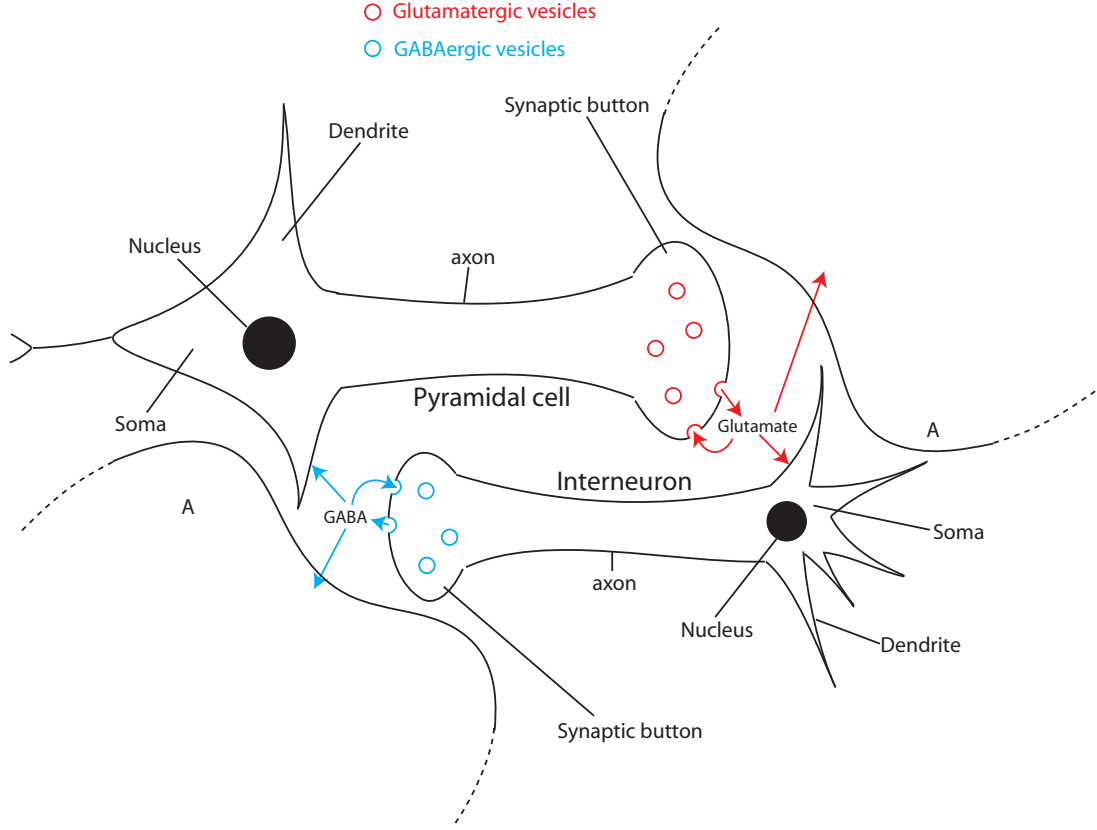


Figure 1: Scheme of neurotransmission mechanisms and neurotransmitter reuptake. Red circles: glutamatergic vesicles. Blue circles: GABAergic vesicles. Red arrows: exchanges of glutamate. Blue arrows: exchanges of GABA. A: astrocytes.

2 Neuro-glia mass approach : bilateral coupling of mesoscopic models

In this section, we briefly recall the structure of the NMM generalizing the Jansen-Rit model and studied in [12], the way to analyze its properties and the predominant time series pattern that it generates. Then we describe the model introduced in [7] to reproduce the glial dynamics. Then we explain our choice of bilateral coupling between these two compartments. Finally, we illustrate its main dynamical differences with the feedforward coupling system (*i.e.* unilateral coupling from the neural compartment upon the glial one).

2.1 Neural mass model and Noise-Induced Spiking

The NMM represents the dynamical interactions between two neural populations at a mesoscopic scale: a main population of pyramidal cells (P) and a population of inhibitory interneurons (I). It also involves the interactions of P with a general population P' representing neighboring pyramidal cells and interacting with P through synaptic connections. There are three feedback loops on population P activity: an inhibitory feedback through the interneuron population I, a direct excitatory feedback of P onto itself (referred to as “direct feedback”) and an indirect excitatory feedback (referred to as “indirect feedback”) involving the population P' (Figure 2(a)).

The conversion process of average pulse density into excitatory and inhibitory postsynaptic potential respectively are based on the following functions introduced by Van Rotterdam *et al.* [35]:

$$\begin{aligned} h_e(t) &= A a t e^{-a t}, \\ h_i(t) &= B b t e^{-b t} \end{aligned}$$

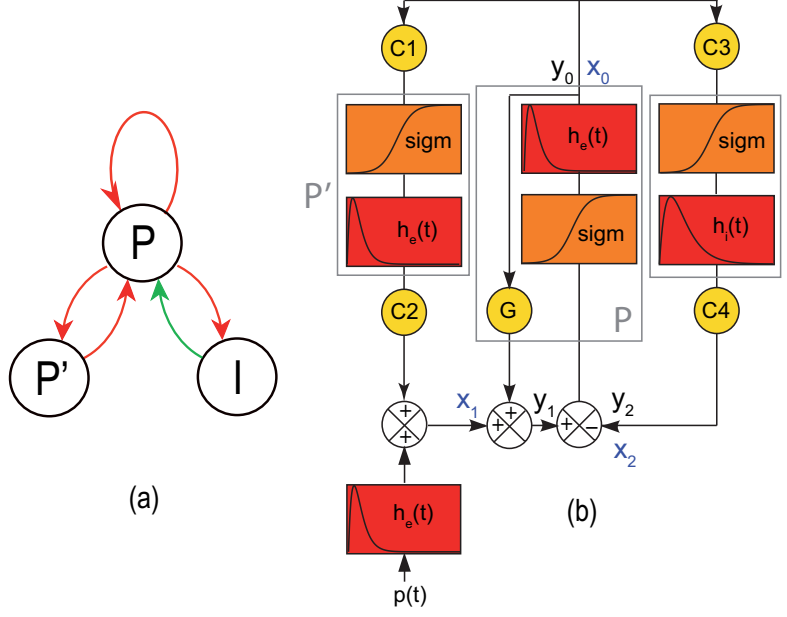


Figure 2: Two schematic representations of the NMM with double excitatory feedbacks. P: main population of pyramidal cells. I: Interneuron population. P': secondary population of pyramidal cells. Red (resp. green) arrows in (a): excitatory (resp. inhibitory) interactions. Box $h_e(t)$ (resp. $h_i(t)$): second order process converting action potentials into excitatory (resp. inhibitory) post-synaptic potential. Box sigm: process converting average membrane potential into average action potential density discharge by neurons of populations P, P' and I respectively. C_i for $i \in \llbracket 1, 4 \rrbracket$: coupling gain parameters depending on the maximal number C of synaptic connections between two populations. G : direct feedback coupling gain. $p(t)$: excitatory input. y_0, y_1, y_2 : state variables. x_0, x_1, x_2 : intermediary variables.

These functions are the basic solutions of the differential operators \mathcal{F}_e and \mathcal{F}_i respectively:

$$\mathcal{F}_e(h_e) = \frac{1}{A} \left(\frac{1}{a} h_e'' - 2 h_e' - a h_e \right) \quad (1a)$$

$$\mathcal{F}_i(h_i) = \frac{1}{B} \left(\frac{1}{b} h_i'' - 2 h_i' - b h_i \right) \quad (1b)$$

In this framework, parameter A (resp. B) tunes the amplitude of excitatory (resp. inhibitory) postsynaptic potentials and $\frac{1}{a}$ (resp. $\frac{1}{b}$) represents the time constant of excitatory (resp. inhibitory) postsynaptic potentials representative of the kinetics of synaptic connections and delays introduced by circuitry of the dendritic tree [11, 35, 19]. Following Freeman's work [11], the sigmoidal functions converting the average membrane potential into an average pulse density have the following form:

$$\text{sigm}(x, v) = \frac{2 e_0}{1 + e^{r(v-x)}}$$

where $2 e_0$ represents the maximum discharge rate, v the excitability threshold and r the sigmoid slope at the inflection point. Finally the NMM receives an excitatory input $p(t)$ standing for the action on population P of neural populations in other areas through long-range synaptic connections. Classically one consider $p(t)$ a gaussian variable to represent a non-specific input and generate the model outputs.

Now we can write the dynamics for the intermediary variables x_0, x_1 and x_2 which represent the outputs of the population P, the population P' and the population I respectively (Figure 2(b)):

$$x_0'' = A a \text{sigm}(x_1 + G x_0 - x_2, v_P) - 2 a x_0' - a^2 x_0 \quad (2a)$$

$$x_1'' = A a C_2 \text{sigm}(C_1 x_0, v_{P'}) - 2 a x_1' - a^2 x_1 + A a p(t) \quad (2b)$$

$$x_2'' = B b C_4 \text{sigm}(C_3 x_0, v_I) - 2 b x_2' - b^2 x_2 \quad (2c)$$

Parameters $C_i, i \in \llbracket 1, 4 \rrbracket$, represent the average number of synapses between two populations. Following [8], each C_i is proportional to the maximal number C of synapses between two populations. The excitation of P by its own output, resulting from the intra-population synaptic connections, is weighted by the coupling gain G .

For sake of comparison, we use a variable change to obtain the same state variables as in the Jansen-Rit model [18] : the excitatory output ($y_0 = x_0$) and the excitatory ($y_1 = x_1 + G x_0$) and inhibitory ($y_2 = x_2$) inputs of the main population P. The output y_0 acts on the secondary pyramidal cell population P' and on the interneuron population I. To analyze the model, we write the dynamics of the state variables y_0, y_1 and y_2 as a system of first order differential equations:

$$y_0' = y_3 \quad (3a)$$

$$y_1' = y_4 \quad (3b)$$

$$y_2' = y_5 \quad (3c)$$

$$y_3' = A a \operatorname{sigm}(y_1 - y_2, v_P) - 2 a y_3 - a^2 y_0 \quad (3d)$$

$$y_4' = A a C_2 \operatorname{sigm}(C_1 y_0, v_{P'}) + A a G \operatorname{sigm}(y_1 - y_2, v_P) - 2 a y_4 - a^2 y_1 + A a p(t) \quad (3e)$$

$$y_5' = B b C_4 \operatorname{sigm}(C_3 y_0, v_I) - 2 b y_5 - b^2 y_2 \quad (3f)$$

In this article, we consider the local field potential (LFP) as the main model output. Following [19], it is defined by $\text{LFP}(t) = y_1(t) - y_2(t)$. It is important to note that, generally, studies of neural mass models, such as Jansen-Rit model, only considered the case with the same constant excitability thresholds for all populations, *i.e.*

$$v_P = v_{P'} = v_I = v_0$$

The behavior of NMMs can be deduced from the bifurcation diagram according to the value $p(t) = p$ considered as a parameter, as it has been performed in [34] on the Jansen-Rit model. In [12], we have classified the types of time series patterns generated by model (3) and the associated bifurcation structures according to the strengths of the different excitative feedbacks applied to population P. Let us recall the bifurcation diagram underlying the predominant type of generated time series, which we will consider in this article.

Model (3) has the following useful particularities that have been highlighted in [12]. First, for a fixed value of parameter p , the y_0 value of a singular point suffices to have explicit expressions of all the other components. Second, for a given y_0 value, there exists a unique value of p such that y_0 corresponds to a singular point. In other terms, the set of singular points obtained for the different values of p is a graph over y_0 . Hence, we can visualize the shape of the singular point locus in the plane (p, y_0) : in the case presented here (see Figure 3), this curve of singular points is S-shaped. In the following description, for a given bifurcation “bif” according to parameter p , we note p_{bif} the bifurcation value and, if the bifurcation involves a singular point, we note y_{bif} the corresponding y_0 value.

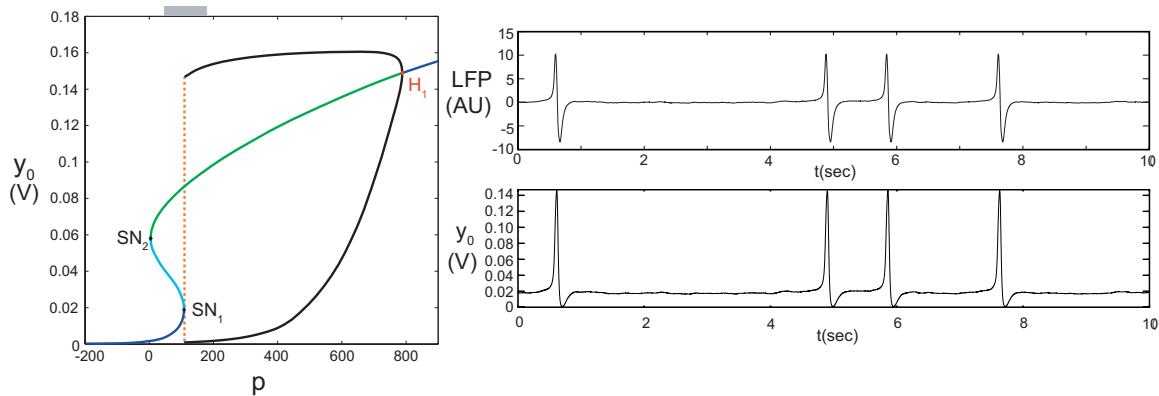


Figure 3: Bifurcation diagram according to p (left) and associated LFP and y_0 time series (right). Blue curves: stable singular points. Cyan (resp. green) curves: singular points with one (resp. two) eigenvalues with positive real parts. Black curves: y_0 extrema along stable limit cycles. Black points (SN₁ and SN₂): saddle-node bifurcations. Red point (H₁): supercritical Hopf bifurcation. Dashed orange line: Saddle-Node on Invariant Circle (SNIC) bifurcation. Horizontal gray bar: confidence interval [$< p > -\sigma, < p > +\sigma$] of the gaussian variable $p(t)$ used to generate the time series.

Two saddle-node bifurcations SN₁ and SN₂ split the curve of singular points into three branches. We name “lower branch”, “middle branch” and “upper branch” the sets of singular points satisfying $y_0 < y_{SN_1}, y_{SN_1} <$

$y_0 < y_{SN_2}$ and $y_0 > y_{SN_2}$ respectively. Singular points on the lower branch are stable (blue) and those on the middle branch are unstable (cyan). Singular points on the upper branch are unstable (green) for $p < p_{H_1}$ and stable (blue) otherwise. At $p = p_{H_1}$ the system undergoes a supercritical Hopf bifurcation H_1 giving birth to a stable limit cycle for $p < p_{H_1}$ that persists until $p = p_{SN_1} = p_{SNIC}$ where it disappears by a saddle-node on invariant circle (SNIC) bifurcation (dashed orange line). The existence of the SNIC bifurcation is essential because it implies the appearance of a large amplitude stable limit cycle with large period. Thereby, according to the value of p , the system alternates between oscillatory phases (for $p > p_{SNIC}$) and quiescent phases (for $p < p_{SNIC}$). In other terms, the value p_{SNIC} plays the role of an activation threshold for the neural compartment, which is a key point of the subsequent analysis.

Note that the oscillation frequency in the generated oscillatory pattern is driven by the value of p : as p tends to p_{SNIC} from above, the limit cycle period tends to infinity. Hence, the closest p is to p_{SNIC} , the lowest is the frequency. Consequently, when considering a gaussian input for the model, the occurrence of spikes and their frequency depend on the features of the normal distribution generating $p(t)$, which led us to refer to the corresponding pattern as Noise-Induced Spiking (NIS) in [12].

Such LFP activity, *i.e.* sparse large amplitude spikes, corresponds to episodic synchronization of the neuron activities among the populations. Physiologically, this pattern of activity arise, as for interictal spiking activity, and is symptomatic of a strong excitability of the neuronal system that can turn into hyperexcitability during pathological crisis. For fixed parameters, the activity is stable in the sense that the oscillation frequency does not change much along time. In the following, we study the variations of the activity when the neural dynamics are altered by the surrounding activity, *i.e.* the glial feedback.

2.2 Glial model : glutamate and GABA concentration dynamics

For reproducing the glial activity, we use the model introduced in [7]. It focuses on the dynamics of glutamate and GABA concentrations, which are the main neurotransmitters of the central nervous system. In [7], the neuro-glial coupling is feedforward: the glial dynamics is driven by the neural activity, generated by the Jansen-Rit model, but does not impact the neural compartment. The model considers the dynamics of glutamate and GABA concentrations, locally to the main population P of pyramidal cells, at different stages of the recycling mechanism. The local nature of this interaction implies that the firing rate of the secondary population P' of pyramidal cells does not impact the glial dynamics associated with the neighboring astrocytes of the main population P. The mechanism is as follows (Figure 4): excited pyramidal cells (*resp.* interneurons) release glutamate (*resp.* GABA) in the extracellular space (synaptic cleft). Astrocytes and pre-synaptic neurons reuptake the neurotransmitters. Astrocytes recycle or consume the neurotransmitters while the presynaptic neurons capture them to complete their stock.

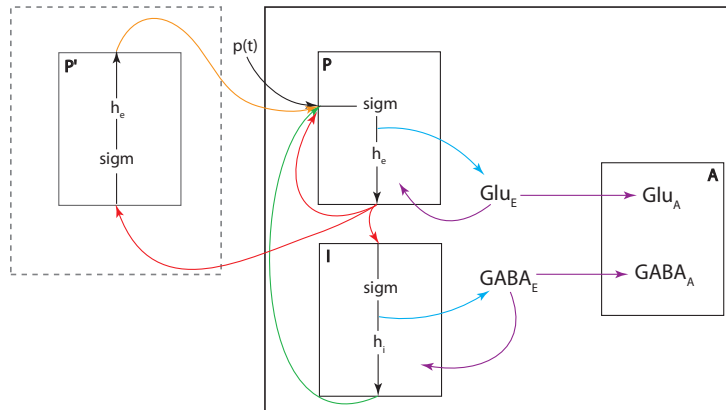


Figure 4: Scheme of the feedforward neuro-glial mass model. P and P': main and secondary populations of pyramidal cells. I: interneuron population. $p(t)$: excitatory input on population P. $[Glu]_E$ and $[GABA]_E$: glutamate and GABA extracellular concentration. $[Glu]_A$ and $[GABA]_A$: glutamate and GABA glial concentrations. Red arrows: $P \rightarrow P$, $P \rightarrow I$ and $P \rightarrow P'$ couplings. Orange arrow: $P' \rightarrow P$ coupling. Green arrow: $I \rightarrow P$ coupling. Cyan arrows: glutamate and GABA release by populations P and I into extracellular space. Purple arrows: glial and neural reuptakes of neurotransmitters.

Following [7] the glial compartment is built on the firing rate (FR_{pyr}) of the pyramidal cell population and the

firing rate (FR_{int}) of the interneuron population. The state variables are

- $[Glu]_{NE}$ and $[GABA]_{IE}$: the fluxes of glutamate and GABA from neurons to extracellular space,
- $[Glu]_E$ and $[GABA]_E$: the neurotransmitter concentrations in the extracellular space,
- $[Glu]_A$ and $[GABA]_A$: the quantity of neurotransmitters recycled and consumed by the astrocytes.

Naturally, the dynamics governing $[Glu]_{NE}$ and $[GABA]_{IE}$ are driven by second-order differential operators similar to the synaptic transfer dynamics introduced in (1) [23, 35]:

$$\begin{aligned}\mathcal{F}_{Glu}(h_{Glu}) &= \frac{1}{W} \left(\frac{1}{w_1} h''_{Glu} - \frac{w_1 + w_2}{w_1} h'_{Glu} - w_2 h_{Glu} \right) \\ \mathcal{F}_{GABA}(h_{GABA}) &= \frac{1}{Z} \left(\frac{1}{z_1} h''_{GABA} - \frac{z_1 + z_2}{z_1} h'_{GABA} - z_2 h_{GABA} \right)\end{aligned}$$

As for the synaptic transfer functions, parameter W (resp. Z) tunes the peak amplitude of glutamate (resp. GABA) concentrations and parameters w_1 and w_2 (resp. z_1 and z_2) tune the rise and decay times of glutamate (resp. GABA) release transfer function. These dynamics are well-suited for reproducing the qualitative and quantitative properties of rise and decay in neurotransmitter concentrations.

The reuptakes of glutamate from the extracellular space by astrocyte ($[Glu]_{EA}$) and neurons ($[Glu]_{EN}$) are triggered when extracellular concentration of glutamate reaches a threshold. Moreover the efficiencies of these processes saturate for high concentrations values, which leads to model these dynamics using sigmoidal functions. GABA reuptakes ($[GABA]_{EA}$ and $[GABA]_{EI}$) are modeled with Michaelis-Menten dynamics following the experimental literature [7]. The dynamics of the extracellular concentrations ($[Glu]_E$ and $[GABA]_E$) are derived from the input and output fluxes described above. The astrocyte concentration dynamics ($[Glu]_A$ and $[GABA]_A$) result from the glial reuptake ones and a linear consumption term.

In sigmoidal functions for $[Glu]_E$ and $[GABA]_E$, parameters V_{glu}^{EA} and V_{glu}^{EN} are the maximal velocities for glutamate reuptakes by the neurons and the astrocytes respectively, s_g represents the activation threshold and r_g the sigmoidal slope at the inflection point. Parameters V_{gba}^{EA} and K_{gba}^{EA} (resp. V_{gba}^{EN} and K_{gba}^{EN}) are respectively the maximal velocity and concentration for glial (resp. neural) GABA transporter. Finally, V_{cglu} and V_{cgba} are the glutamate and GABA degradation rates in astrocytes. We refer the reader to [7] for a detailed explanation of the dynamics.

Hence, the feedforward model obtained by coupling the NMM defined by (3) and the glial dynamics introduced in [7] reads

$$y'_0 = y_3 \tag{4a}$$

$$y'_1 = y_4 \tag{4b}$$

$$y'_2 = y_5 \tag{4c}$$

$$y'_3 = A a \text{sigm}(y_1 - y_2, v_P) - 2 a y_3 - a^2 y_0 \tag{4d}$$

$$y'_4 = A a C_2 \text{sigm}(C_1 y_0, v_P) + A a G \text{sigm}(y_1 - y_2, v_P) - 2 a y_4 - a^2 y_1 + A a p(t) \tag{4e}$$

$$y'_5 = B b C_4 \text{sigm}(C_3 y_0, v_I) - 2 b y_5 - b^2 y_2 \tag{4f}$$

$$[Glu]_{NE}' = d[Glu]_{NE} \tag{4g}$$

$$d[Glu]_{NE}' = W w_1 \text{sigm}(y_1 - y_2, v_P) - (w_1 + w_2) d[Glu]_{NE} - w_1 w_2 [Glu]_{NE} \tag{4h}$$

$$[Glu]_E' = [Glu]_{NE} - \frac{V_{glu}^{EA}}{1 + e^{r_g s_g - r_g [Glu]_E}} - \frac{V_{glu}^{EN}}{1 + e^{r_g s_g - r_g [Glu]_E}} \tag{4i}$$

$$[Glu]_A' = \frac{V_{glu}^{EA}}{1 + e^{r_g s_g - r_g [Glu]_E}} - V_{cglu} [Glu]_A \tag{4j}$$

$$[GABA]_{IE}' = d[GABA]_{IE} \tag{4k}$$

$$d[GABA]_{IE}' = Z z_1 \text{sigm}(C_3 y_0, v_I) - (z_1 + z_2) d[GABA]_{IE} - z_1 z_2 [GABA]_{IE} \tag{4l}$$

$$[GABA]_E' = [GABA]_{IE} - \frac{V_{gba}^{EA}}{K_{gba}^{EA} + [GABA]_E} [GABA]_E - \frac{V_{gba}^{EN}}{K_{gba}^{EN} + [GABA]_E} [GABA]_E \tag{4m}$$

$$[GABA]_A' = \frac{V_{gba}^{EA}}{K_{gba}^{EA} + [GABA]_E} [GABA]_E - V_{cgba} [GABA]_A \tag{4n}$$

Table 1 specifies the parameter values used for the simulations in the following sections. The values of parameters associated with the NMM have been chosen to reproduce NIS behavior using the analysis in [12].

Neurons		Glutamate	GABA
$A = 3.25 \text{ mV}$	$C = 135$	$W = 53.6 \mu\text{M}\cdot\text{s}^{-1}$	$Z = 53.6 \mu\text{M}\cdot\text{s}^{-1}$
$B = 22 \text{ mV}$	$\alpha_1 = 1$	$w_1 = 90 \text{ s}^{-1}$	$z_1 = 90 \text{ s}^{-1}$
$a = 100 \text{ s}^{-1}$	$\alpha_2 = 0.8$	$w_2 = 33 \text{ s}^{-1}$	$z_2 = 33 \text{ s}^{-1}$
$b = 50 \text{ s}^{-1}$	$\alpha_3 = 0.25$	$V_{\text{glu}}^{\text{EA}} = 4.5 \mu\text{M}\cdot\text{s}^{-1}$	$V_{\text{gba}}^{\text{EA}} = 2 \mu\text{M}\cdot\text{s}^{-1}$
$e_0 = 2.5 \text{ s}^{-1}$	$\alpha_4 = 0.25$	$V_{\text{glu}}^{\text{EN}} = 0.5 \mu\text{M}\cdot\text{s}^{-1}$	$K_{\text{gba}}^{\text{EA}} = 8 \mu\text{M}$
$v_0 = 6 \text{ mV}$	$G = 40$	$r_g = 0.9 \mu\text{M}^{-1}$	$V_{\text{gba}}^{\text{EN}} = 5 \mu\text{M}\cdot\text{s}^{-1}$
$r = 0.56 \text{ mV}^{-1}$		$s_g = 6 \mu\text{M}$	$K_{\text{gba}}^{\text{EN}} = 24 \mu\text{M}$
		$V_{\text{cglu}} = 9 \mu\text{M}\cdot\text{s}^{-1}$	$V_{\text{cgba}} = 9 \mu\text{M}\cdot\text{s}^{-1}$

Table 1: Values of the neuro-glia model parameters.

System (4) is built as a feedforward coupling of the neural compartment onto the glial one. Hence, in this model, the neural compartment is not impacted by the neurotransmitter concentrations in the extracellular space. As mentioned in the introduction, these concentrations have been proven to modulate the local neuron excitability and this feedback has been identified in recent studies [1] to be an essential mechanism of several pathologies triggered by glial reuptake deficiencies. Consequently, our aim is to include such feedback in the model in order to study the effects of different astrocyte dysfunctioning on the neuronal activity.

2.3 Glial feedback and neuro-glia mass model

The concentrations of neurotransmitters in a synaptic cleft act on the excitability threshold of the post-synaptic neuron. In the neuro-glia model (4) the alteration of this neural excitability threshold can be reproduced by dynamical changes in v_P , $v_{P'}$ and v_I . In the following, we describe how we model the modulation of the neuron excitability in each population by the neurotransmitter concentrations in the extracellular space basing ourselves on biological knowledge.

Extracellular concentrations of neurotransmitters have a thresholded impact on neural activity [1]. Precisely, on one hand, the concentrations must be large enough to impact significantly the neural activity. On the other hand, the postsynaptic neurons are saturated when these concentrations become to large and, consequently, the neural excitability remains bounded. It is worth noticing that quantitative experimental data of the impact of neurotransmitter concentrations on neural excitability do not exist up to now. By default, we consider sigmoidal functions to model the glial feedback on neural excitability which is a natural choice for aggregating the qualitative experimental knowledge. Yet the upcoming mathematical analysis can be easily extended to any bounded increasing functions with a unique inflection point.

We introduce three sigmoidal functions to model the components of the glial feedback: Si_{Glup} for the glutamate feedback on pyramidal cells, Si_{GluI} for the glutamate feedback on interneurons and Si_{GABA} for the GABA feedback on pyramidal cells. We parameterize these functions as follows

$$\text{Si}_{\text{Glup}}([\text{Glu}]_{\text{E}}) = \frac{m_{\text{Glup}}}{1 + e^{r_{\text{Glup}}(v_{\text{Glup}} - [\text{Glu}]_{\text{E}})}} \quad (5a)$$

$$\text{Si}_{\text{GluI}}([\text{Glu}]_{\text{E}}) = \frac{m_{\text{GluI}}}{1 + e^{r_{\text{GluI}}(v_{\text{GluI}} - [\text{Glu}]_{\text{E}})}} \quad (5b)$$

$$\text{Si}_{\text{GABA}}([\text{GABA}]_{\text{E}}) = \frac{m_{\text{GABA}}}{1 + e^{r_{\text{GABA}}(v_{\text{GABA}} - [\text{GABA}]_{\text{E}})}} \quad (5c)$$

The parameter values used for the simulations in the following sections are given in Table 2 and have been chosen to reproduce an average physiological behavior.

$m_{\text{Glup}} = 2.5$	$m_{\text{GluI}} = 1$	$m_{\text{GABA}} = 1$
$r_{\text{Glup}} = 0.15$	$r_{\text{GluI}} = 0.15$	$r_{\text{GABA}} = 0.12$
$v_{\text{Glup}} = 30$	$v_{\text{GluI}} = 30$	$v_{\text{GABA}} = 25$

Table 2: Parameter values of the sigmoidal function $\text{Si}_{\text{GluI}}([\text{Glu}]_{\text{E}})$, $\text{Si}_{\text{Glup}}([\text{Glu}]_{\text{E}})$ and $\text{Si}_{\text{GABA}}([\text{GABA}]_{\text{E}})$.

We note that the fixation mechanisms of glutamate on pyramidal cells and interneurons are the same since the neurotransmitter transporters are independent on the type of neuron. Thus, only parameters m_{Glu_p} and m_{Glu_i} representing the maximal coupling gains of the glutamate-related component of the glial feedback discriminate between the coupling functions Si_{Glu_p} and Si_{Glu_i} , since the synaptic sensitivities may not be the same in pyramidal cells and interneurons.

At the beginning of this subsection, we evoked that the glial feedback acts on the excitability thresholds of neurons. More specifically, if there is an excess of neurotransmitter in a synapse from a neuron n_1 of population N_1 to a neuron n_2 of population N_2 , the extracellular concentration of neurotransmitter acts on the postsynaptic neuron n_2 by changing its excitability threshold. In system (4) the excitability threshold of neurons, that is a parameter at the individual scale, does not appear explicitly. However, when the excitability of the population N_2 neurons changes at the individual scale, the number of neurons activated in this population by a given input changes as well and thus the output of this population is also modified. Consequently, we choose to change parameter v_{N_2} in the equation corresponding to the output of population N_2 since this parameter represents a modulation of the threshold of the sigmoidal function sigm .

Let us now describe how we build the feedbacks on the dynamics of the neural compartment using the sigmoidal functions of the neurotransmitter concentrations introduced in (5). We need to consider separately each type of synapse in the NMM, and the variables x_0 , x_1 and x_2 for the feedbacks building. The NMM embeds five types of synaptic connections between populations:

- S_1 from P' to P,
- S_2 from P to P',
- S_3 from P to I,
- S_4 from I to P,
- S_5 from P to itself

In the following we detail the modulation of neural intermediary variables for each kind of synapse separately, then we gather these changes to specify the coupling terms reproducing the glial feedback.

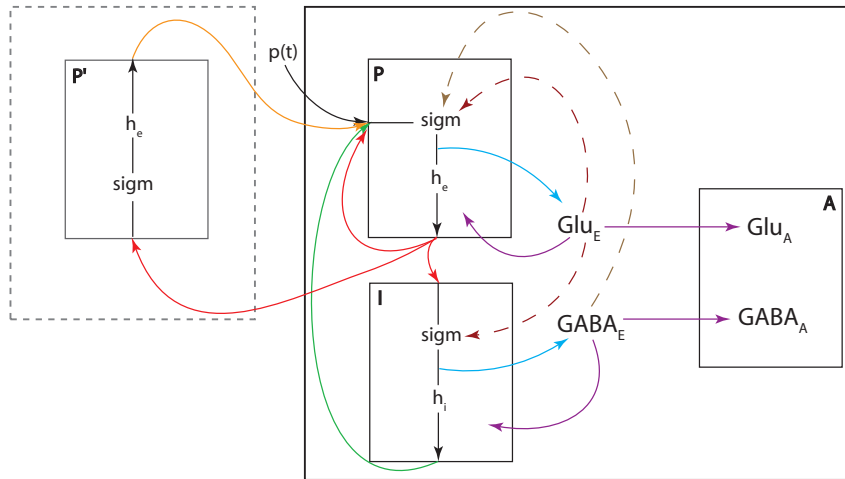


Figure 5: Neuro-glial model with glial feedback. P and P': main and secondary populations of pyramidal cells. I: interneuron population. $p(t)$: excitatory input on population P. $[\text{Glu}]_E$ and $[\text{GABA}]_E$: glutamate and GABA extracellular concentrations. $[\text{Glu}]_A$ and $[\text{GABA}]_A$: glutamate and GABA glial concentrations. Red arrows: P→P, P→I and P→P' couplings. Orange arrow: P'→P coupling. Green arrow: I→P coupling. Cyan arrows: glutamate and GABA release by populations P and I into extracellular space. Purple arrows: glial and neural reuptakes of neurotransmitters. Red dashed arrows: glutamate feedbacks on populations P and I. Brown dashed arrow: GABA feedback on population P.

In the framework of the local neuro-glial mass model, the glial feedback does not impact the synaptic connections of type S_1 or S_2 . As a matter of fact, the glial compartment only takes into account neurotransmitters

released locally by neurons of populations P and I, whereas population P' is non local to population P. Hence, extracellular concentrations of neurotransmitters in the vicinity of P' have no impact on the neuronal activity of P and the concentrations in the neighborhood of P and I do not influence postsynaptic neurons of population P'. In the discussion, we evoke the fact that network models based on the local model presented in this article may naturally take into account such modulation of mid-range synaptic connections. In the current study focusing on the local model, we consider the case of constant $v_{P'} = v_0$.

A synaptic connection of type S_3 concerns the variable x_2 . In case of glutamate excess in the extracellular space, the postsynaptic neuron is more excitable. Consequently, more neurons are activated in the population I. We model this mechanism by introducing a dependency of population I excitability threshold v_I on the extracellular glutamate concentration and set in equation (2c) :

$$v_I = v_0 - \text{Si}_{\text{Glu}_I}([\text{Glu}]_E).$$

On one hand, a synaptic connection of type S_4 is concerned by extracellular concentrations of GABA since it involves GABAergic interneurons. In case of a GABA excess in the extracellular space, the inhibition of the postsynaptic neuron is strengthened, *i.e.* less neurons are activated in population P which is translated in the NMM by an increase of the threshold of the sigmoidal term in the x_0 dynamics. On the other hand, a synaptic connection of type S_5 is impacted by the extracellular concentration of glutamate implying a modulation of variable x_0 dynamics as well. In case of an excess of glutamate in this kind of synapse, the postsynaptic neuron is more excitable. Hence, more neurons are activated in population P which can be reproduced by a decrease in the threshold parameter appearing in (2a). Gathering both modulations impacting the excitability of population P, we set in equation (2a)

$$v_P = v_0 + \text{Si}_{\text{GABA}}([\text{GABA}]_E) - \text{Si}_{\text{Glu}_P}([\text{Glu}]_E).$$

The new neuro-glial mass model embedding the glial feedback is obtained from model (4) by considering the dynamical entries v_I and v_P mentioned above. Accordingly, the sigmoidal functions appearing in equations (4d), (4e), (4f), (4h) and (4l) become:

$$\begin{aligned} \text{sigm}(y_1 - y_2, v_P) &= \frac{2 e_0}{1 + e^{r(v_0 + \text{Si}_{\text{GABA}}([\text{GABA}]_E) - \text{Si}_{\text{Glu}_P}([\text{Glu}]_E) - (y_1 - y_2))}} \\ \text{sigm}(C_1 y_0, v_{P'}) &= \frac{2 e_0}{1 + e^{r(v_0 - C_1 y_0)}} \\ \text{sigm}(C_3 y_0, v_I) &= \frac{2 e_0}{1 + e^{r(v_0 - \text{Si}_{\text{Glu}_I}([\text{Glu}]_E) - C_3 y_0)}} \end{aligned}$$

2.4 Effect of a GABA bolus : an illustration of the glial feedback impact

We compare time series generated by the neuro-glial model with and without glial feedback to illustrate its impact on the model behavior (Figure 6). To this aim, we mimic the same GABA bolus injection (20 AU) in the extracellular space at $t = 30s$ with both models. For obtaining regular patterns and ease the comparison between the outputs, we consider a constant input $p(t) = p$ with a value of p close to and greater than p_{SNIC} (Figures 6, panels (a1) and (b1)). Hence, from initial time to $t = 30s$, both model generate pacemaker NIS oscillations at a low frequency. Note that, even if GABA concentration is low and the corresponding sigmoidal feedback is consequently very weak, it already impacts the neural activity, which implies a difference in the spike frequency between the two LFP time series.

In the time series generated by the model without feedback (left panels of Figure 6), the neural activity and the glutamate concentration dynamics remain unchanged (Figure 6(a)) after the artificial and instantaneous increase in $[\text{GABA}]_E$ that aims to mimic a GABA bolus injection. In contrast, in the model with glial feedback (right panels of Figure 6), the strong increase in GABA concentration implies a break in neural activity, and thus a decrease in glutamate concentration. Once GABA concentration has become sufficiently low, neural activity starts again. The glutamate and GABA concentrations come back to their respective basal lines and oscillate under the effect of the neural spikes.

These phenomenons can be explained using bifurcation-based arguments (top panels of Figure 6). In the system without feedback, the neural dynamics is entirely decoupled from the glial one. Hence, the bifurcation diagram of the NMM remains unchanged during all the simulation (Figure 6(a1)). On the other hand, in the system with feedback, the bifurcation diagram of the neural system is deformed along time, in particular the value of p_{SNIC} changes with the glial variables. Consequently, right after the GABA bolus, p_{SNIC} becomes greater than the input value p (Figure 6(b2)). Moreover, we recall that p_{SNIC} plays the role of an activation threshold. Thus, as long as

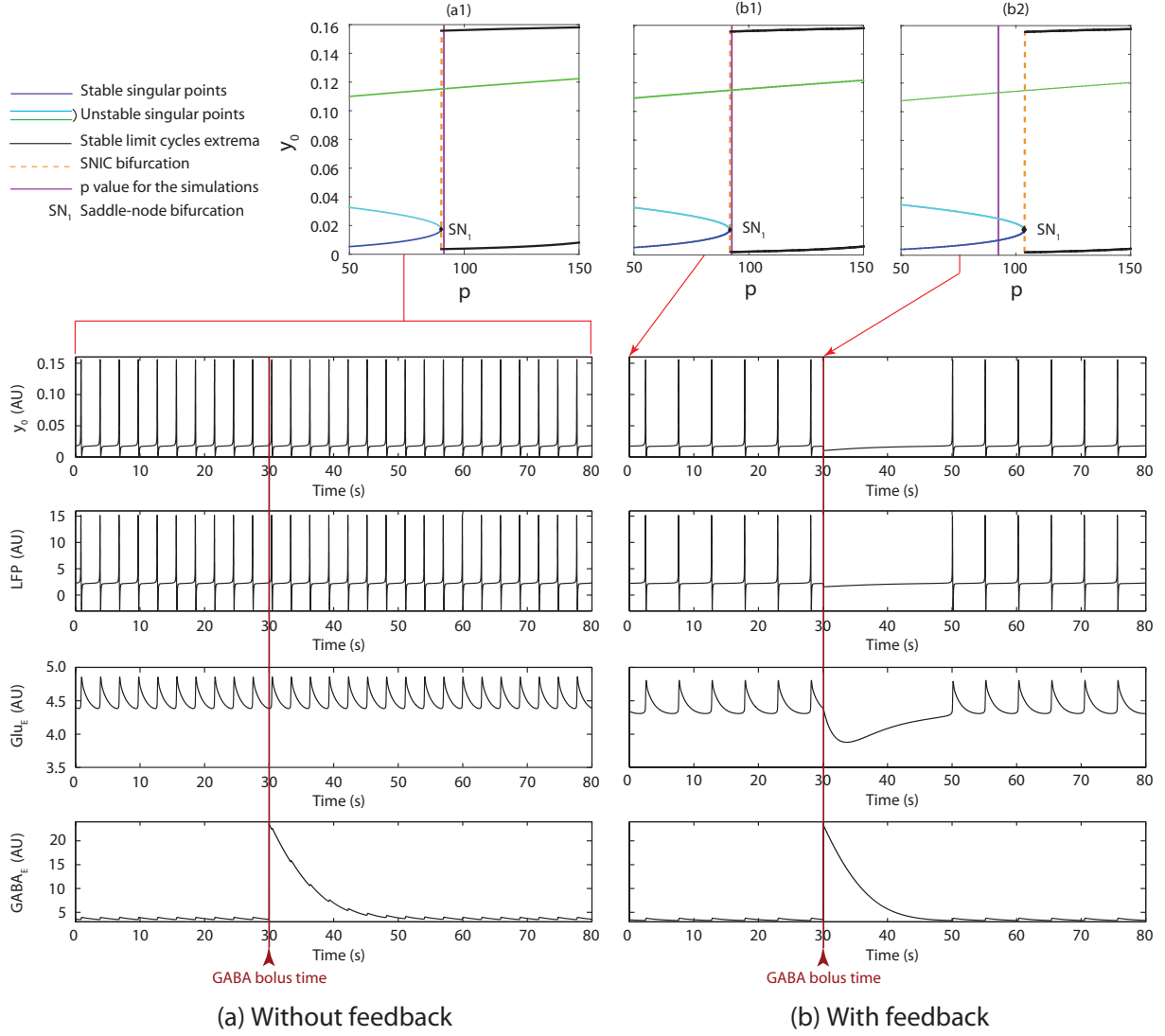


Figure 6: Bifurcation diagrams according to p (top panels) computed for the model without feedback for all t (a1) and for the model with feedback at $t = 0s$ (b1) and $t = 30s$ (b2). Time series (bottom panels) corresponding to y_0 , LFP, extracellular concentrations of Glutamate and GABA generated by the models without feedback (left) and with feedback (right). The purple lines on the bifurcation diagrams materialize the fixed value of input p . The dark red lines on the time series materialize the time of GABA bolus injection

GABA concentration remains high, the neural variables are at steady state and the neural compartment remains quiescent. A direct calculation shows that the glial compartment has a single stable singular point : extracellular GABA concentration decreases towards this attractive state implying a slow decrease in p_{SNIC} . Once, GABA concentration is low enough, p_{SNIC} becomes smaller than p , and the system oscillates again.

This analysis shows how the model with feedback can take into account changes in glutamate and GABA dynamics to modify all the dynamics of the system and illustrates the interest of embedding the glial feedback in such neuro-glial model. Our model allows us to study the effects of variations in glutamate or GABA dynamics on neural activity. In the following, we study the effects of deficiencies in the reuptake of neurotransmitters by the astrocytes both on extracellular concentrations and neural activity. For both types of deficiency (GABA and glutamate), we first describe the biologic context and mechanisms and their outcomes, then we provide a mathematical analysis of the underlying dynamical mechanisms to explain the effects that can be expected in the biological system.

3 GABA glial deficiency

We consider an astrocyte presenting a deficiency in its GABA transporters which implies a low capacity to reuptake the extracellular GABA. A glial cell is linked with several neurons, more specifically with several synapses. Thus the GABA in synaptic clefts linked with the defective astrocyte increases. Consequently, the concerned post-synaptic neurons receive more inhibition from the extracellular GABA and release less neurotransmitters in the following synapses. Thus, considering several defective glial cells, all neurons in a local neighborhood are affected. In summary, when glial cells present a deficiency in GABA reuptake, local neurons are more inhibited, and we expect a decrease of their activities in the corresponding simulations.

In the model, parameter $V_{\text{gba}}^{\text{EA}}$ stands for the maximum velocity of the GABA flux from the extracellular space to the astrocytes, *i.e.* in case of GABA saturation in the extracellular space. In that sense, it is related to the efficiency of the main glial transporter of GABA and modulates the glial reuptake dynamics. Consequently, to simulate a deficiency in the GABA glial reuptake, we decrease the value of this parameter. At the neuronal level we are interested in p_{SNIC} value according to the feedback sigmoidal functions. For sake of simplicity in this mathematical analysis, we set:

$$\begin{aligned} \text{Si}_{\text{Glu}}([\text{Glu}]_{\text{E}}) &\rightarrow v_1 \\ \text{Si}_{\text{Glu}}([\text{Glu}]_{\text{E}}) &\rightarrow \frac{m_{\text{Glu}}}{m_{\text{Glu}}} v_1 \\ \text{Si}_{\text{GABA}}([\text{GABA}]_{\text{E}}) &\rightarrow v_2 \end{aligned}$$

The ranges of v_1 and v_2 are defined by the limits of $\text{Si}_{\text{Glu}}([\text{Glu}]_{\text{E}})$ and $\text{Si}_{\text{GABA}}([\text{GABA}]_{\text{E}})$ respectively:

$$v_1 \in [0, m_{\text{Glu}}] \text{ and } v_2 \in [0, m_{\text{GABA}}]$$

With these new notations, the dynamical excitability thresholds v_{P} , $v_{\text{P}'}$ and v_{I} of populations P, P' and I become:

$$\begin{aligned} v_{\text{P}} &= v_0 + v_2 - \frac{m_{\text{Glu}}}{m_{\text{Glu}}} v_1 \\ v_{\text{P}'} &= v_0 \\ v_{\text{I}} &= v_0 - v_1 \end{aligned}$$

With these new parameters, an increase or a decrease in GABA (resp. glutamate) extracellular concentration is represented by an increase or a decrease in the value of v_2 (resp. v_1) respectively. The natural effect of a deficiency of GABA glial reuptake on neural activity is an increase in the extracellular GABA concentration. Thereby, we characterize the dependency of p_{SNIC} on the value of v_2 . The assumption that v_1 can be kept constant is justified in the following Remark 3.1.

Proposition 3.1. p_{SNIC} is linear and increasing according to v_2

Proof. The set of the system singular points obtained for the different values of parameter p can be explicitly expressed according to y_0 , v_1 and v_2 all other parameters being fixed. The y_0 components of the singular points for given values of p , v_1 and v_2 are characterized as solutions of

$$p = f(y_0, v_1, v_2) \tag{6}$$

where

$$\begin{aligned} f(y_0, v_1, v_2) &= \frac{a}{A} \left(v_0 - \frac{m_{\text{Glu}}}{m_{\text{Glu}}} v_1 + v_2 \right) - \frac{a}{A r} \ln \left(\frac{2 A e_0 - a y_0}{a y_0} \right) - C_2 \text{sigm}(C_1 y_0, v_0) \\ &\quad + \frac{a B}{b A} C_4 \text{sigm}(C_3 y_0, v_0 - v_1) - \frac{a G}{A} y_0. \end{aligned} \tag{7}$$

All the other components of a given singular point result by direct calculation from its y_0 component. We rewrite equation (7) as follows

$$f(y_0, v_1, v_2) = \frac{a}{A} v_2 + q(y_0, v_1) \tag{8}$$

Obviously the two saddle-node bifurcation values p_{SN_1} and p_{SN_2} are local extrema of function $f(y_0, v_1, v_2)$. In particular $p_{\text{SN}_1} = p_{\text{SNIC}}$ is the local maximum of $f(y_0, v_1, v_2)$ and is defined as the solution of

$$p = f(y_0, v_1, v_2) \quad (9a)$$

$$\frac{\partial f}{\partial y_0}(y_0, v_1, v_2) = 0 \quad (9b)$$

$$\frac{\partial^2 f}{\partial y_0^2}(y_0, v_1, v_2) \leq 0 \quad (9c)$$

Since $\frac{\partial f}{\partial y_0}(y_0, v_1, v_2)$ is independent on v_2 , so is y_{SNIC} and it can be considered as a parameter in equation (9a). From (8) and (9) we obtain the following expression for p_{SNIC}

$$p_{\text{SNIC}} = \frac{a}{A} v_2 + q(y_{\text{SNIC}}, v_1)$$

□

Let us consider the model generating an oscillatory output with a fixed value of p ($p_{\text{SNIC}} < p$). If the extracellular concentration of GABA increases (e.g. by an injection of a GABA bolus as in Figure 6), the value of v_2 increases and Proposition 1 asserts that the value of p_{SNIC} also increases. As already explained, the closest p_{SNIC} is to p , with $p_{\text{SNIC}} < p$, the largest is the limit cycle period, thus the oscillation frequency of the outputs decreases. If p_{SNIC} increases enough such that $p_{\text{SNIC}} > p$, the stable limit cycle of the system disappears, and the neural compartment becomes quiescent.

In the case of a deficiency of GABA glial reuptake, the extracellular concentration of GABA increases, and we can use Proposition 1 to explain the subsequent effects. For that, we use the following *in silico* protocol: we initialize the neuro-glial model in an oscillatory phase with a low oscillation frequency and consider $p(t)$ a Gaussian input. At $t = 40s$, we turn off the GABA glial reuptake by setting $V_{\text{gba}}^{\text{EA}} = 0$ (Figure 7). The result is an increase in GABA extracellular concentration implying an increase in p_{SNIC} . As p_{SNIC} increases, the probability for $p(t)$ to overcome p_{SNIC} along the associated brownian motion decreases, and also does the oscillation frequency (Figure 7). Consequently, we observe a decrease in the oscillation frequency after $t > 40s$. In the time series, the oscillation frequency decreases gradually during a transient ($40s < t < 60s$) until reaching its minimum. This can be explained by the slow increase of GABA extracellular concentration that reaches its new baseline at $t = 60s$.

Remark 3.1. A deficiency in the GABA reuptake by the astrocyte implies a decrease in the neural activity. Hence, the glutamate extracellular concentration remains close to the baseline. Consequently, the impact of the changes in v_1 value can be neglected and, under this approximation, Proposition 3.1 characterizes the global effect of such deficiency on the neural compartment excitability.

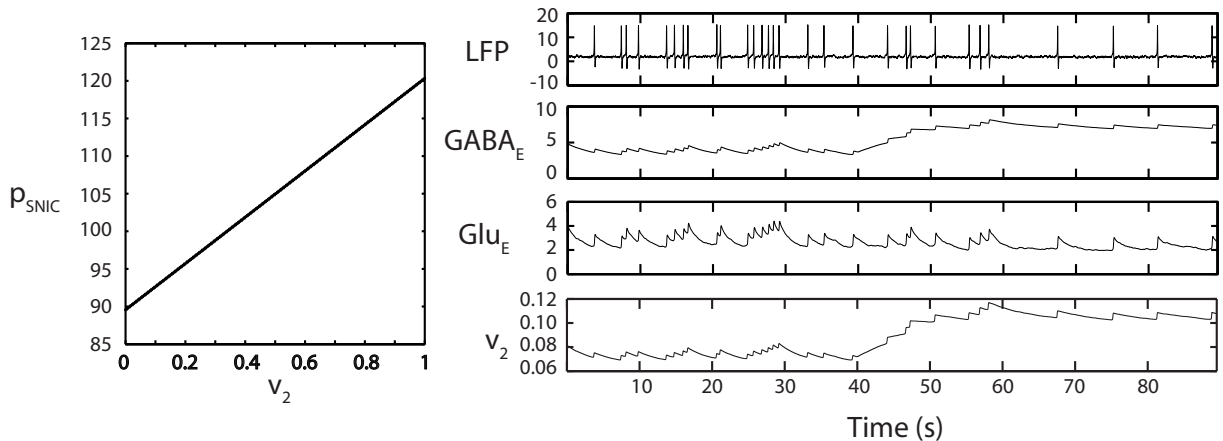


Figure 7: Variation of p_{SNIC} value according to v_2 (left). Time series corresponding to LFP, $[\text{GABA}]_E$, $[\text{Glu}]_E$ and $v_2 = \text{Si}_{\text{GABA}}([\text{GABA}]_E)$ (right from top to bottom) for $p(t)$ a Gaussian variable. At $t = 40s$, the GABA glial reuptake is artificially altered by setting $V_{\text{gba}}^{\text{EA}} = 0$.

4 Glutamate glial deficiency

In this section, we investigate the impact of a deficiency of glutamate reuptake by the astrocytes upon the neuronal activity. Such deficiency provoke an increase in the extracellular concentration of glutamate and, consequently, neurons in this neighborhood are more excitable. Yet, it is important to note that interneurons release more GABA implying an increase in the GABA extracellular concentration as well, and an enhancement of the inhibition of the pyramidal activity. Hence, the possible balance between glutamate-induced over-excitation and subsequent GABA-induced over-inhibition may lead to different types of response of the neuronal compartment. As previously, for studying theoretically the underlying mechanisms, we consider the NMM with two parameters v_1 and v_2 representing glutamate- and GABA-related feedbacks respectively. In the last section, we have characterized the linearity of p_{SNIC} according to v_2 for any fixed value of v_1 . Now, let us fix the value of v_2 and study the variations of p_{SNIC} according to v_1 .

We recall that p_{SNIC} is a key value of the system structure since it represents the excitability threshold of the neural compartment. It is important to note that in a specific case, the SNIC bifurcation disappears without disappearance of this excitability threshold. In this case, the supercritical Hopf bifurcation occurring for a large value of p and the saddle-node bifurcation (SN_1) previously linked to the SNIC bifurcation, are preserved and a subcritical Hopf bifurcation appears, close to SN_1 , giving birth to an unstable limit cycle. This limit cycle persists for a very small interval of p values before it disappears through a fold bifurcation of limit cycles. We refer the reader to [12] for more details about this bifurcation structure. For certain parameter values of the whole model, the bifurcation structure may therefore be lost when v_1 varies. Computing the region of the parameter space (of high dimension) for which it remains unchanged for any v_1 is difficult. Yet, the previous analysis of the NMM [12] ensures us that this region is large. Thus, in the following, we assume that p_{SNIC} exists and the associated saddle-node bifurcation is not degenerated for all $v_1 \in [0, m_{\text{Glu}}]$, *i.e.* the maximal interval of values taken by $v_1 = \text{Si}_{\text{Glu}}([\text{Glu}]_{\text{E}})$, which is the case, in particular, for the parameter values given in Table 1 and 2, that have been used for the simulations.

We recall that p_{SNIC} can be written as follows:

$$p_{\text{SNIC}} = f(y_{\text{SNIC}}, v_1, v_2) \quad (10)$$

where f is given by (7). Since we consider v_2 fixed we introduce the function

$$g(y_0, v_1) \equiv f(y_0, v_1, v_2)|_{v_2 \text{ fixed}}$$

As explained above, for each v_1 , there exists a unique bifurcation value p_{SNIC} occurring at the non-hyperbolic (saddle-node) singular point characterized by y_{SNIC} which is defined by

$$\begin{cases} \frac{\partial g}{\partial y_0}(y_{\text{SNIC}}, v_1) = 0, \\ \frac{\partial^2 g}{\partial y_0^2}(y_{\text{SNIC}}, v_1) < 0. \end{cases}$$

This value satisfies $p_{\text{SNIC}} = g(y_{\text{SNIC}}, v_1)$. We can not find the explicit expressions of $y_{\text{SNIC}}(v_1)$ and $p_{\text{SNIC}}(v_1)$. Thus, for characterizing the variations of p_{SNIC} with v_1 , we take advantage of the implicit definitions above and focus on localizing the extrema of $p_{\text{SNIC}}(v_1)$.

Proposition 4.1. Assume that for all $v_1 \in [0, m_{\text{Glu}}]$, p_{SNIC} exists and the associated saddle-node bifurcation is not degenerate. Then

1. if $\frac{m_{\text{Gluup}}}{m_{\text{Glu}}} \geq \frac{B e_0 r C_4}{2b}$, $p_{\text{SNIC}}(v_1)$ has no local extremum,
2. if $\frac{m_{\text{Gluup}}}{m_{\text{Glu}}} \in]0, \frac{B e_0 r C_4}{2b}[$, $p_{\text{SNIC}}(v_1)$ may admit two local extrema: a minimum at v_1^* and a maximum at v_1^{**} .
If both exist, then $v_1^* < v_1^{**}$.

Proof. Let us search for local extrema of function $p_{\text{SNIC}}(v_1)$ which is implicitly defined by (9). Hence, we are interested in solving the following problem of optimization under constraint :

$$\min / \max \left\{ g(y_0, v_1) \mid \frac{\partial g}{\partial y_0}(y_0, v_1) = 0 \right\} \quad (11)$$

We introduce the associated lagrangian function

$$L(y_0, v_1, \lambda) = g(y_0, v_1) - \lambda \frac{\partial g}{\partial y_0}(y_0, v_1)$$

The necessary condition for the existence of an extremum of g under the constraint $\frac{\partial g}{\partial y_0} = 0$ is

$$\vec{\nabla} L(y_0, v_1, \lambda) = 0$$

that is

$$\frac{\partial g}{\partial y_0}(y_0, v_1) - \lambda \frac{\partial^2 g}{\partial y_0^2}(y_0, v_1) = 0, \quad (12a)$$

$$\frac{\partial g}{\partial v_1}(y_0, v_1) - \lambda \frac{\partial^2 g}{\partial v_1 \partial y_0}(y_0, v_1) = 0, \quad (12b)$$

$$\frac{\partial g}{\partial y_0}(y_0, v_1) = 0. \quad (12c)$$

By assumption, the saddle-node bifurcation associated with the SNIC bifurcation is not degenerate, *i.e.* every solution of (11) for $v_1 \in [0, m_{\text{Glui}}]$ satisfies $\frac{\partial^2 g}{\partial y_0^2}(y_0, v_1) \neq 0$. Thus, system (12) reads

$$\lambda = 0, \quad (13a)$$

$$\frac{\partial g}{\partial v_1}(y_0, v_1) = 0, \quad (13b)$$

$$\frac{\partial g}{\partial y_0}(y_0, v_1) = 0. \quad (13c)$$

Consequently, if the problem under constraint admits an extremum, this extremum satisfies $\frac{\partial g}{\partial v_1} = 0$. Following the assumption that a SNIC bifurcation occurs for any value of $v_1 \in [0, m_{\text{Glui}}]$, equation (13c) admits a solution for any v_1 . Hence, if the problem under constraint admits an extremum, it corresponds to a SNIC bifurcation occurring at (y_0, v_1) such that

$$\frac{\partial g}{\partial y_0}(y_0, v_1) = 0.$$

From (7), we obtain

$$\frac{\partial g}{\partial v_1}(y_0, v_1) = -\frac{a}{A} \left(\frac{m_{\text{Glup}}}{m_{\text{Glui}}} + \frac{B}{b} C_4 \frac{\partial \text{sigm}}{\partial v}(C_3 y_0, v_0 - v_1) \right).$$

Using the facts that, for any fixed values of y_0 , function $v_1 \rightarrow \frac{\partial g}{\partial v_1}(y_0, v_1)$ is bell-shaped and its maximal value does not depend on y_0 (see Figure 8), one obtains that function $\frac{\partial g}{\partial v_1}(y_0, v_1)$ vanishes in v_1 if

$$\frac{m_{\text{Glup}}}{m_{\text{Glui}}} \in \left] 0, \frac{B e_0 r C_4}{2b} \right]. \quad (14)$$

If $\frac{m_{\text{Glup}}}{m_{\text{Glui}}} \geq \frac{B e_0 r C_4}{2b}$, function $\frac{\partial g}{\partial v_1}(y_0, v_1)$ admits no zero, which proves the first item of the Proposition 2.

Now, we assume that condition (14) is fulfilled and we search the values of v_1 satisfying $\frac{\partial g}{\partial v_1}(y_0, v_1) = 0$, *i.e.*

$$\frac{m_{\text{Glup}}}{m_{\text{Glui}}} + \frac{B}{b} C_4 \frac{\partial \text{sigm}}{\partial v}(C_3 y_0, v_0 - v_1) = 0.$$

which reads

$$\left(e^{r(v_0 - v_1 - C_3 y_0)} \right)^2 \frac{m_{\text{Glup}}}{m_{\text{Glui}}} + e^{r(v_0 - v_1 - C_3 y_0)} \left(2 \frac{m_{\text{Glup}}}{m_{\text{Glui}}} - 2 \frac{B}{b} e_0 r C_4 \right) + \frac{m_{\text{Glup}}}{m_{\text{Glui}}} = 0. \quad (15)$$

Setting

$$V_{\pm} = \frac{B e_0 r C_4 - b \frac{m_{\text{Glup}}}{m_{\text{Glui}}} \pm \sqrt{(B e_0 r C_4)^2 - 2 B e_0 r C_4 \frac{m_{\text{Glup}}}{m_{\text{Glui}}}}}{b \frac{m_{\text{Glup}}}{m_{\text{Glui}}}} \quad (16)$$

we obtain the two solutions $v^* < v^{**}$ of $\frac{\partial g}{\partial v_1}(y_0, v_1) = 0$:

$$v_1^* = v_0 - C_3 y_0 - \frac{1}{r} \ln(V_+) \quad (17)$$

$$v_1^{**} = v_0 - C_3 y_0 - \frac{1}{r} \ln(V_-) \quad (18)$$

Note that v_1^* (resp. v_1^{**}) corresponds to the extremum when the saddle-node SN_1 (resp. SN_2) crosses the fold of the surface $g(y_0, v_1) = p$. We consider $v_1 = v_1^*$ and we note y_0^* the value of y_0 corresponding to the SNIC connection for this value of v_1 , *i.e.* the solution of

$$\begin{aligned}\frac{\partial g}{\partial y_0}(y_0, v_1^*) &= 0 \\ \frac{\partial^2 g}{\partial y_0^2}(y_0, v_1^*) &< 0\end{aligned}$$

To prove that p_{SNIC} reaches a local minimum at $v_1 = v_1^*$, we introduce the bordered Hessian matrix \bar{H} associated with the lagrangian function at its singular point $(y_0, v_1, \lambda) = (y_0^*, v_1^*, 0)$ (solution of system (13)):

$$\bar{H}(y_0^*, v_1^*, 0) = \begin{pmatrix} 0 & \frac{\partial^2 g}{\partial y_0^2} & \frac{\partial^2 g}{\partial v_1 \partial y_0} \\ \frac{\partial^2 g}{\partial y_0^2} & \frac{\partial^2 L}{\partial y_0^2} & \frac{\partial^2 L}{\partial v_1 \partial y_0} \\ \frac{\partial^2 g}{\partial v_1 \partial y_0} & \frac{\partial^2 L}{\partial v_1 \partial y_0} & \frac{\partial^2 L}{\partial v_1^2} \end{pmatrix}_{|(y_0^*, v_1^*, 0)} = \begin{pmatrix} 0 & \frac{\partial^2 g}{\partial y_0^2} & \frac{\partial^2 g}{\partial v_1 \partial y_0} \\ \frac{\partial^2 g}{\partial y_0^2} & \frac{\partial^2 g}{\partial y_0^2} & \frac{\partial^2 g}{\partial v_1 \partial y_0} \\ \frac{\partial^2 g}{\partial v_1 \partial y_0} & \frac{\partial^2 g}{\partial v_1 \partial y_0} & \frac{\partial^2 g}{\partial v_1^2} \end{pmatrix}_{|(y_0^*, v_1^*, 0)}$$

The determinant of $\bar{H}(y_0^*, v_1^*, 0)$ is given by

$$\det \bar{H}(y_0^*, v_1^*, 0) = -\frac{\partial^2 g}{\partial y_0^2}(y_0^*, v_1^*) \left[\frac{\partial^2 g}{\partial y_0^2}(y_0^*, v_1^*) \frac{\partial^2 g}{\partial v_1^2}(y_0^*, v_1^*) - \left(\frac{\partial^2 g}{\partial v_1 \partial y_0}(y_0^*, v_1^*) \right)^2 \right]$$

On one hand, the saddle-node associated with the SNIC bifurcation is not degenerate and is a local maximum of $g(y_0, v_1)$, thus $\frac{\partial^2 g}{\partial y_0^2}(y_0^*, v_1^*) < 0$. On the other hand, for any $y_0, v_1 \rightarrow \frac{\partial g}{\partial v_1}(y_0, v_1)$ is increasing at (y_0, v_1^*) (see Figure 8), thus $\frac{\partial^2 g}{\partial v_1^2}(y_0^*, v_1^*) > 0$. Finally

$$\det \bar{H}(y_0^*, v_1^*, 0) < 0$$

and (y_0^*, v_1^*) corresponds to a local minimum of p_{SNIC} . A similar argument proves that (y_0^{**}, v_1^{**}) corresponds to a local maximum of p_{SNIC} (where y_0^{**} is the y_0 value corresponding to SN_2 bifurcation for $v_1 = v_1^{**}$). \square

The above proposition can be interpreted as a necessary condition for having a change in the sense of variations of p_{SNIC} when v_1 varies in $[0, m_{\text{glui}}]$. The following result gives a sufficient condition for v_1^* actually lying in $[0, m_{\text{glui}}]$.

Corollary 4.1. We have $v_1^* \in [0, m_{\text{Glui}}]$ if and only if $\frac{m_{\text{Glup}}}{m_{\text{Glui}}} \in [I_1, I_2]$ where

$$I_1 = \frac{2 B e_0 r C_4}{b} \frac{e^{r(v_0 - C_3 y_0^*)}}{(1 + e^{r(v_0 - C_3 y_0^*)})^2}, \quad (19)$$

$$I_2 = \frac{2 B e_0 r C_4}{b} \frac{e^{r(v_0 - m_{\text{Glui}} - C_3 y_0^*)}}{(1 + e^{r(v_0 - m_{\text{Glui}} - C_3 y_0^*)})^2} \quad (20)$$

Proof. Since v_1^* satisfies $\frac{\partial g}{\partial v_1}(y_0^*, v_1^*) = 0$, one obtains, from equation (15),

$$\frac{m_{\text{Glup}}}{m_{\text{Glui}}} = \frac{2 B e_0 r C_4}{b} \frac{e^{r(v_0 - v_1^* - C_3 y_0^*)}}{(1 + e^{r(v_0 - v_1^* - C_3 y_0^*)})^2} = h(v_1^*) \quad (21)$$

For any y_0 , function $v_1 \mapsto \frac{e^{r(v_0 - v_1 - C_3 y_0)}}{(1 + e^{r(v_0 - v_1 - C_3 y_0)})^2}$ is strictly increasing over $[0, m_{\text{Glui}}]$ and $v_1^* \in [0, m_{\text{Glui}}]$ if and only if $\frac{m_{\text{Glup}}}{m_{\text{Glui}}} \in [I_1, I_2]$ defined by (19) and (20) (see Figure 8). \square

In conclusion, for a fixed value of v_2 , p_{SNIC} reaches a local minimum at a value $v_1^* \in [0, m_{\text{Glui}}]$ if and only if

$$\frac{m_{\text{Glup}}}{m_{\text{Glui}}} \in \left] 0, \frac{B e_0 r C_4}{2b} \left[\cap [I_1, I_2].$$

Moreover, in section 3 about the GABA glial deficiency, we proved that, for a fixed value of v_1 , p_{SNIC} is linear and increasing with v_2 . Both results allow us to predict that there exist three shapes of $p_{\text{SNIC}}(v_1, v_2)$ according to the value of $\frac{m_{\text{Glup}}}{m_{\text{Glui}}}$.

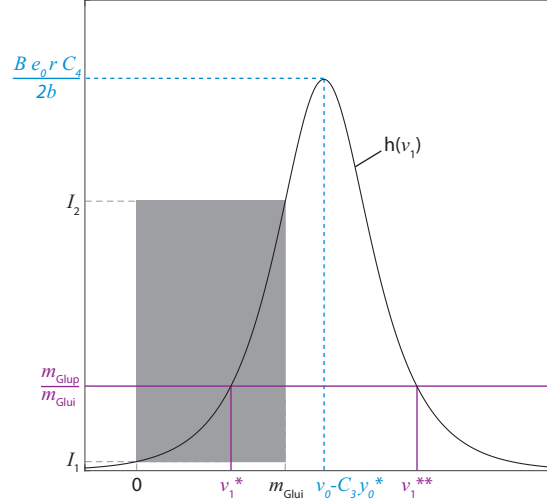


Figure 8: Graphic representation of function h defined by (21) and interval $[I_1, I_2]$ for which $v_1^* \in [0, m_{\text{glui}}]$.

- If $\frac{m_{\text{Glu}_{up}}}{m_{\text{Glu}_i}} < I_1$ then $v_1^* < 0$ and p_{SNIC} strictly increases with v_1 and v_2 .
- If $\frac{m_{\text{Glu}_{up}}}{m_{\text{Glu}_i}} > I_2$, then $v_1^* > m_{\text{Glu}_i}$ and p_{SNIC} strictly decreases when v_1 increases (for v_2 fixed) and strictly increases with v_2 (for v_1 fixed).
- If $\frac{m_{\text{Glu}_{up}}}{m_{\text{Glu}_i}} \in [I_1, I_2]$, then $v_1^* \in [0, m_{\text{Glu}_i}]$ and p_{SNIC} decreases when v_1 increases in $[0, v_1^*]$ and increases with $v_1 > v_1^*$ (for v_2 fixed).

In the following we illustrate the three qualitative types of neural activity resulting from an astrocyte deficiency to capture glutamate using the following values :

$$a) \quad \frac{m_{\text{Glu}_{up}}}{m_{\text{Glu}_i}} = 1.7 < I_1, \quad b) \quad \frac{m_{\text{Glu}_{up}}}{m_{\text{Glu}_i}} = 3.2 > I_2, \quad c) \quad \frac{m_{\text{Glu}_{up}}}{m_{\text{Glu}_i}} = 2.43 \in [I_1, I_2]$$

For each case, we provide simulations representing the value of p_{SNIC} in (v_1, v_2) space and time series generated by the model when the glutamate glial reuptake is altered (Figures 9, 10 and 11).

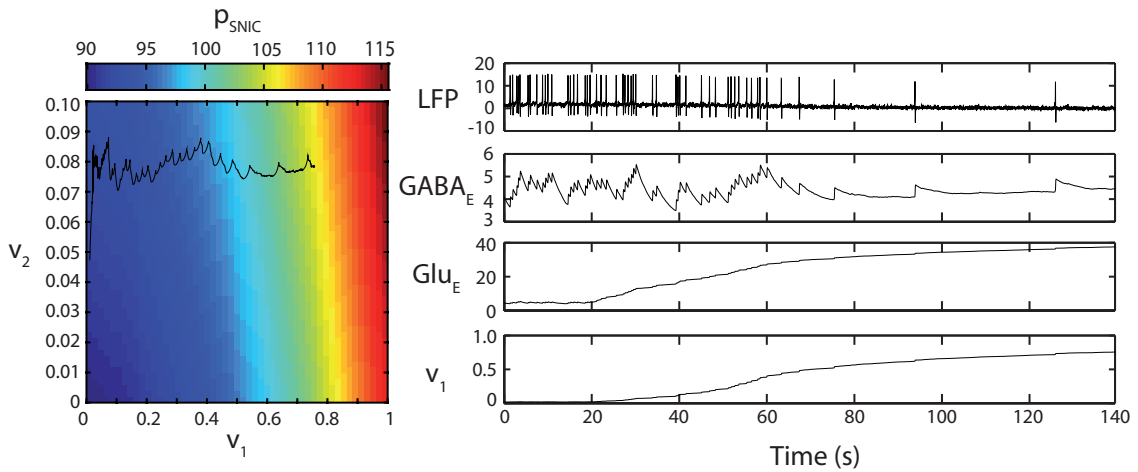


Figure 9: Colormap displaying the value of p_{SNIC} in $(v_1, v_2) \in [0, 1] \times [0, 0.1]$ space (left panel), and time series corresponding to LFP, $[\text{GABA}]_E$, $[\text{Glu}]_E$ and $v_1 = \text{Si}_{\text{Glu}_i}([\text{Glu}]_E)$ (right panels) obtained with $\frac{m_{\text{Glu}_{up}}}{m_{\text{Glu}_i}} = 1.7$. Black curve on the colormap: trace of $(\text{Si}_{\text{Glu}_i}([\text{Glu}]_E), \text{Si}_{\text{GABA}}([\text{GABA}]_E))$ along the orbits. At $t = 20s$, we alter the glutamate glial reuptake by setting $V_{\text{glu}}^{\text{EA}} = 0$.

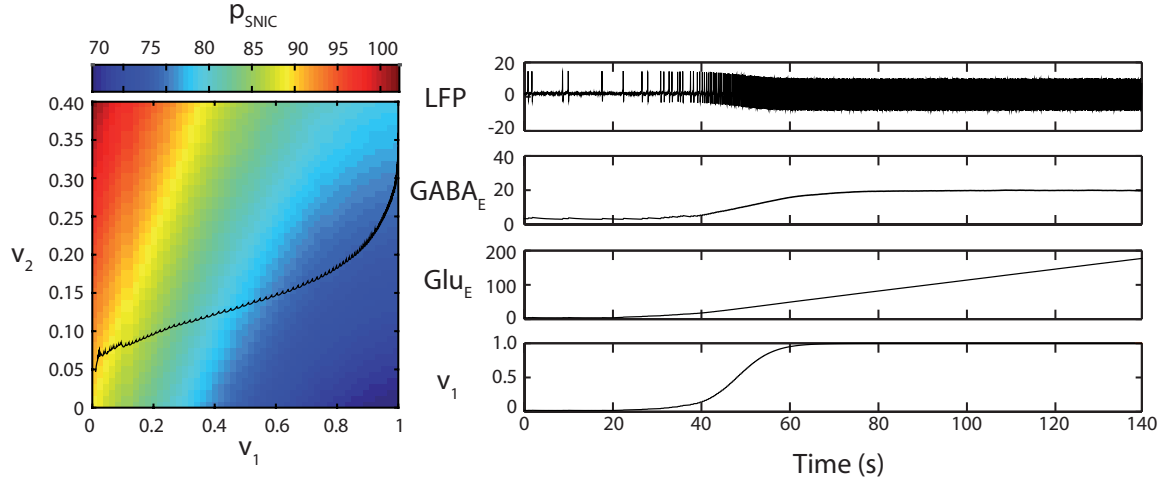


Figure 10: Colormap displaying the value of p_{SNIC} in $(v_1, v_2) \in [0, 1] \times [0, 0.4]$ space (left panel), and time series corresponding to LFP, $[\text{GABA}]_E$, $[\text{Glu}]_E$ and $v_1 = \text{Si}_{\text{Glu}}([\text{Glu}]_E)$ (right panels) obtained with $\frac{m_{\text{Glu}}}{m_{\text{Glu}}} = 3.2$. Black curve on the colormap: trace of $(\text{Si}_{\text{Glu}}([\text{Glu}]_E), \text{Si}_{\text{GABA}}([\text{GABA}]_E))$ along the orbits. At $t = 20\text{s}$, we alter the glutamate glial reuptake by setting $V_{\text{glu}}^{\text{EA}} = 0$.

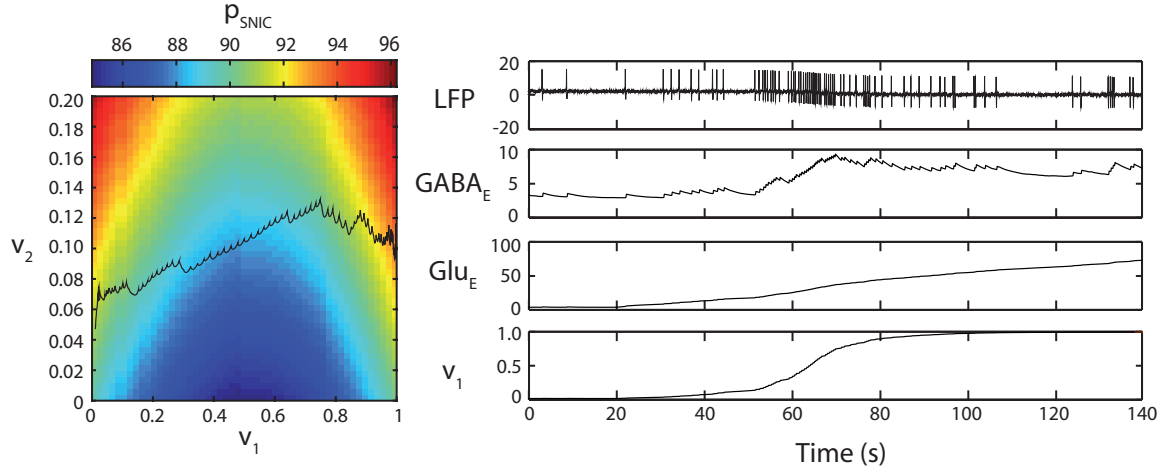


Figure 11: Colormap displaying the value of p_{SNIC} in $(v_1, v_2) \in [0, 1] \times [0, 0.2]$ space (left panel), and time series corresponding to LFP, $[\text{GABA}]_E$, $[\text{Glu}]_E$ and $v_1 = \text{Si}_{\text{Glu}}([\text{Glu}]_E)$ (right panels) obtained with $\frac{m_{\text{Glu}}}{m_{\text{Glu}}} = 2.43$. Black curve on the colormap: trace of $(\text{Si}_{\text{Glu}}([\text{Glu}]_E), \text{Si}_{\text{GABA}}([\text{GABA}]_E))$ along the orbits. At $t = 20\text{s}$, we alter the glutamate glial reuptake by setting $V_{\text{glu}}^{\text{EA}} = 0$.

For $\frac{m_{\text{Glu}}}{m_{\text{Glu}}} = 1.7 < I_1$ (case *a*), figure 9), v_1^* is negative and thus p_{SNIC} increases with v_1 . Thereby, when we reproduce a glutamate glial deficiency triggering an increase in v_1 value, we observe a decrease in the oscillation frequencies in the neural activity. Moreover, reduction of the glutamate glial reuptake together with the strong decrease of neural activity, triggers an increase in the baseline of glutamate extracellular concentration. Indeed, the lack of reuptake involves the accumulation of extracellular glutamate. Since neurons are less activated, the glutamate release is lowered and the neural reuptake can stabilize the glutamate extracellular concentration.

Figure 10 illustrates case *b*) ($\frac{m_{\text{Glu}}}{m_{\text{Glu}}} = 3.2 > I_2$). Since $v_1^* > 1$, p_{SNIC} decreases as v_1 increases. Thereby, a glutamate glial deficiency triggers an increase of v_1 value, and we observe an increase in the oscillation frequencies in the neural time-series. Since the glial reuptake is reduced, glutamate accumulates in the extracellular space and the corresponding concentration baseline increases drastically.

Figure 11 illustrates intermediary case *c*) ($\frac{m_{\text{Glu}}}{m_{\text{Glu}}} = 2.43 \in [I_1, I_2]$). Since $v_1^* \in]0, 1[$, p_{SNIC} decreases for $v_1 < v_1^*$ and increases otherwise. Thereby, when we simulate a glutamate glial deficiency triggering an increase in

v_1 value, we observe an increase in the oscillation frequencies in LFP time series, followed by a decrease. Indeed, after the alteration of the glutamate glial reuptake, the glutamate extracellular concentration increases and excites more pyramidal cells and interneurons. Subsequently, interneurons release more GABA, which implies an increase of the inhibition of pyramidal cells and a decrease in the neural activity. This sequence of events explains the delay in the regulation of the oscillation frequencies.

This kind of behavior is physiologically relevant. Indeed, it is conceivable that an excess of glutamate extracellular concentration is regulated after a delay, triggering a decrease of neural activity after the initial increase. Moreover, the frequency after the regulation delay can be greater or lower than the initial one, depending on the value of the ratio $\frac{m_{\text{GluP}}}{m_{\text{GluI}}}$. Note that this value can be tuned to obtain v_1^* small enough and p_{SNIC} large enough so that the frequency after regulation is equal or lower than the one before reuptake deficiency. This property offers the possibility of fitting the model outputs to experimental data and allows us to propose hypotheses about physiological and pathological mechanisms.

5 Conclusion and Discussion

In this article, we have introduced a new neuro-glial mass model built on a bilateral coupling of the NMM studied in [12] and the glial model proposed in [7] focusing on GABA and glutamate concentration dynamics. The model is based on recent biological knowledge resulting from experimental data [6, 17, 26, 28] to ground the interaction between the neural and extracellular/glial compartments. Note that, as explained in the beginning of section 2.2., only basic properties of the dynamical coupling are needed to prove the qualitative dependencies studied in sections 3 and 4. By lack of experimental data in the literature, we chose sigmoidal functions for relaying the glial feedbacks in the simulations because they represent a paragon of bounded increasing functions involving a significant threshold effect. Then, using the interpretation of the aggregated – yet biophysical – parameters involved in this model, we have reproduced *in silico* various types of deficiencies in the reuptake of GABA or Glutamate by the astrocytes and studied their impact upon the neural activity. We took advantage of the bifurcation analysis performed in [12] to characterize theoretically the dynamical mechanism leading to local neuronal hyperexcitability through a modulation of the SNIC bifurcation standing for the excitability threshold of the neural compartment.

The first result concerns the impact of a deficiency in the reuptake of GABA by astrocytes which implies an increase in the GABA concentration in the extracellular space. We have shown (Proposition 1) that the excitability threshold p_{SNIC} increases linearly with the feedback term value depending on the GABA concentration in the extracellular space. Hence, such an astrocyte deficiency simulated in the model results in a decrease in the frequency of neural activity, which is consistent with the biological knowledge [9, 22]. The second result concerns the neuronal response to a deficiency in the reuptake of Glutamate by the astrocytes. In this case, the neural activity may either be reduced or enhanced or, alternatively, may experience a transient of high activity before stabilizing around a new activity state with a frequency close to the nominal one (*i.e.* before induction of astrocyte deficiency). We have characterized (Proposition 2 and Corollary 1) the relationships between parameters of the model for predicting the neuronal response. It is worth noticing that it is possible to calculate explicitly the SNIC bifurcation for the uncoupled NMM (see [12]), but not for the bilaterally coupled model embedding the glial compartment. Hence, we have expressed the question of characterizing the variations in the neuronal excitability as an optimization problem under an equality constraint resulting from the implicit characterization of the saddle-node bifurcation.

The two model parameters m_{GluP} and m_{GluI} involved in Proposition 2 and Corollary 1 represent the maximal strengths of the Glutamate concentration impacts on the excitability of the pyramidal cell and the interneuron populations respectively. Our model-based study shows that the neural compartment may “resist” to the impact of glutamate excess in the extracellular space only if the value of $\frac{m_{\text{gluP}}}{m_{\text{gluI}}}$ lies in a positive interval. For small values ($\frac{m_{\text{gluP}}}{m_{\text{gluI}}} < I_1$), the neural activity frequency is lowered, as shown in Figure 9, while, for high values ($\frac{m_{\text{gluP}}}{m_{\text{gluI}}} > I_2$), the activity frequency increases drastically and permanently, as shown in Figure 10. For intermediary values, the neural activity recovers after a high frequency transient to a comparable mode despite the high values of extracellular Glutamate and GABA concentrations. Note that I_1 and I_2 explicitly depend on the coupling strength modulating the inhibition of the pyramidal cells activity by the interneurons (*i.e.* parameter C_4). On the other hand, only I_2 depends on m_{GluI} . Hence, one might interpret this later dependency as a balance between the Glutamate-related glial feedbacks upon pyramidal cells and interneuron that the system should fulfill for being able to recover from a dysfunction in the astrocyte activity and avoid hyper-excitable behaviors.

An interesting fact should be noticed for future experimental investigation based on this study: for $\frac{m_{\text{gluP}}}{m_{\text{gluI}}} > I_1$, the astrocyte deficiency in capturing Glutamate induces, in addition to the increase in the extracellular Glutamate concentration, an increase in the GABA concentration, even greater than the one resulting from a default in GABA

capture. Dynamically, this increase is necessary so that the system could reach an alternative state and recover a low frequency activity, but may not be sufficient if the glial feedback on the pyramidal cells and the interneurons is unbalanced, *i.e.* for to large values of $\frac{m_{glup}}{m_{glui}}$. The GABA increase induced by an excess of extracellular Glutamate and the corresponding neuronal response form an experimental benchmark to identify the mechanism of the transition through hyperexcitability and potential neuronal recovery.

Future theoretical works will extend the analysis of the local neuro-glial dynamical interactions by studying the model response when the neuronal compartment undergoes a drastic change in its bifurcation structure induced by a deficiency in the astrocyte compartment dynamics. As a matter of fact, for other parameter values corresponding to different inter- and intra-population connectivity strengths, the neural compartment may generate other types of time series than Noise-Induced Spiking (NIS) among those identified in [12]. Therefore, the present study can be continued to study the dynamical mechanisms underlying successive transitions through various activity regimes. Another perspective will consist to consider two coupled neuro-glial models, the input $p(t)$ in each one being replaced by the output of the other one. The extension of the results presented in this article to such a system may provide useful methodological tools to tackle the hectic question of neuro-glial network modeling.

Acknowledgements

This work was performed within the Labex SMART (ANR-11-LABX-65) supported by French state funds managed by the ANR within the Investissements d’Avenir program under reference ANR-11-IDEX-0004-02. We thank H. Berry for helpful comments on this work. We also thank S. Blanchard and F. Wendling for allowing us to use the glial model they submitted.

References

- [1] A. Araque, V. Parpura, R. P. Sanzgiri, and P. G. Haydon. Glutamate-dependent astrocyte modulation of synaptic transmission between cultured hippocampal neurons. *The European Journal of Neuroscience*, 10(6):2129–2142, June 1998.
- [2] A. Araque, V. Parpura, R. P. Sanzgiri, and P. G. Haydon. Tripartite synapses: glia, the unacknowledged partner. *Trends in Neurosciences*, 22(5):208–215, May 1999.
- [3] A. Aubert and R. Costalat. A model of the coupling between brain electrical activity, metabolism, and hemodynamics: application to the interpretation of functional neuroimaging. *NeuroImage*, 17(3):1162–1181, Nov. 2002.
- [4] A. Aubert and R. Costalat. Interaction between astrocytes and neurons studied using a mathematical model of compartmentalized energy metabolism. *Journal of cerebral blood flow and metabolism: official journal of the International Society of Cerebral Blood Flow and Metabolism*, 25(11):1476–1490, Nov. 2005.
- [5] A. Aubert, R. Costalat, P. J. Magistretti, and L. Pellerin. Brain lactate kinetics: Modeling evidence for neuronal lactate uptake upon activation. *Proceedings of the National Academy of Sciences of the United States of America*, 102(45):16448–16453, Nov. 2005.
- [6] C. Bellone, C. Lüscher, and M. Mamei. Mechanisms of synaptic depression triggered by metabotropic glutamate receptors. *Cellular and molecular life sciences: CMLS*, 65(18):2913–2923, Sept. 2008.
- [7] S. Blanchard, S. Sallet, A. Ivanov, P. Benquet, C. Benar, H. Benali, and F. Wendling. The neuro-glio-vascular coupling through a new computational model: astrocytes activation can explain the Cerebral Blood Flow nonlinear response to interictal events. *Submitted*.
- [8] V. Braitenberg and A. Schüz. *Cortex: Statistics and Geometry of Neuronal Connectivity*. Springer, 2nd edition, 1998.
- [9] S. G. Brickley and I. Mody. Extrasynaptic GABA(A) receptors: their function in the CNS and implications for disease. *Neuron*, 73(1):23–34, Jan. 2012.
- [10] M. De Pittà, V. Volman, H. Berry, and E. Ben-Jacob. A tale of two stories: astrocyte regulation of synaptic depression and facilitation. *PLoS computational biology*, 7(12):e1002293, Dec. 2011.

- [11] W. Freeman. *Mass action in the nervous system*. Academic Press, New York, 1975.
- [12] A. Garnier, A. Vidal, C. Huneau, and H. Benali. A neural mass model with direct and indirect excitatory feedback loops: identification of bifurcations and temporal dynamics. *Neural Computation*, 27:329–364, 2015.
- [13] C. Giaume, A. Koulakoff, L. Roux, D. Holcman, and N. Rouach. Astroglial networks: a step further in neuroglial and gliovascular interactions. *Nature Reviews. Neuroscience*, 11(2):87–99, Feb. 2010.
- [14] R. Gruetter, E. R. Seaquist, and K. Ugurbil. A mathematical model of compartmentalized neurotransmitter metabolism in the human brain. *American Journal of Physiology. Endocrinology and Metabolism*, 281(1):E100–112, July 2001.
- [15] M. M. Halassa, T. Fellin, and P. G. Haydon. The tripartite synapse: roles for gliotransmission in health and disease. *Trends in Molecular Medicine*, 13(2):54–63, Feb. 2007.
- [16] M. M. Halassa and P. G. Haydon. Integrated brain circuits: astrocytic networks modulate neuronal activity and behavior. *Annual Review of Physiology*, 72:335–355, 2010.
- [17] Y. H. Huang, S. R. Sinha, K. Tanaka, J. D. Rothstein, and D. E. Bergles. Astrocyte glutamate transporters regulate metabotropic glutamate receptor-mediated excitation of hippocampal interneurons. *The Journal of Neuroscience: The Official Journal of the Society for Neuroscience*, 24(19):4551–4559, May 2004.
- [18] B. H. Jansen and V. G. Rit. Electroencephalogram and visual evoked potential generation in a mathematical model of coupled cortical columns. *Biological Cybernetics*, 73(4):357–366, 1995.
- [19] B. H. Jansen, G. Zouridakis, and M. E. Brandt. A neurophysiologically-based mathematical model of flash visual evoked potentials. *Biological Cybernetics*, 68(3):275–283, 1993.
- [20] P. Kowianski, G. Lietzau, A. Steliga, M. Waskow, and J. Morys. The astrocytic contribution to neurovascular coupling—still more questions than answers? *Neuroscience research*, 75(3):171–183, 2013.
- [21] G. Losi, M. Cammarota, and G. Carmignoto. The Role of Astroglia in the Epileptic Brain. *Frontiers in Pharmacology*, 3, July 2012.
- [22] B. Luscher, T. Fuchs, and C. L. Kilpatrick. GABAA receptor trafficking-mediated plasticity of inhibitory synapses. *Neuron*, 70(3):385–409, May 2011.
- [23] B. Molaee-Ardekani, J. Márquez-Ruiz, I. Merlet, R. Leal-Campanario, A. Gruart, R. Sánchez-Campusano, G. Birot, G. Ruffini, J.-M. Delgado-García, and F. Wendling. Effects of transcranial Direct Current Stimulation (tDCS) on cortical activity: A computational modeling study. *Brain Stimulation*, 6(1):25–39, Jan. 2013.
- [24] S. Nadkarni and P. Jung. Modeling synaptic transmission of the tripartite synapse. *Physical Biology*, 4(1):1–9, Mar. 2007.
- [25] S. Nadkarni, P. Jung, and H. Levine. Astrocytes optimize the synaptic transmission of information. *PLoS computational biology*, 4(5):e1000088, May 2008.
- [26] C. M. Niswender and P. J. Conn. Metabotropic glutamate receptors: physiology, pharmacology, and disease. *Annual Review of Pharmacology and Toxicology*, 50:295–322, 2010.
- [27] V. Parpura and P. G. Haydon. Physiological astrocytic calcium levels stimulate glutamate release to modulate adjacent neurons. *Proceedings of the National Academy of Sciences of the United States of America*, 97(15):8629–8634, July 2000.
- [28] C. Pittenger, M. H. Bloch, and K. Williams. Glutamate abnormalities in obsessive compulsive disorder: neurobiology, pathophysiology, and treatment. *Pharmacology & Therapeutics*, 132(3):314–332, Dec. 2011.
- [29] D. Postnov, R. Koreshkov, N. Brazhe, A. Brazhe, and O. Sosnovtseva. Dynamical patterns of calcium signaling in a functional model of neuron-astrocyte networks. *Journal of Biological Physics*, 35(4):425–445, Oct. 2009.

- [30] D. Postnov, L. Yazanova, and O. Sosnovtseva. Functional modeling of neural-glia interaction. *BioSystems*, 89(1-3):84–91, May 2007.
- [31] A. Schousboe, L. Bak, and H. Waagepetersen. Astrocytic control of biosynthesis and turnover of the neurotransmitters glutamate and gaba. *Frontiers in endocrinology*, 4:102, 2013.
- [32] G. Seifert, K. Schilling, and C. Steinhäuser. Astrocyte dysfunction in neurological disorders: a molecular perspective. *Nature Reviews. Neuroscience*, 7(3):194–206, Mar. 2006.
- [33] A. N. Silchenko and P. A. Tass. Computational modeling of paroxysmal depolarization shifts in neurons induced by the glutamate release from astrocytes. *Biological Cybernetics*, 98(1):61–74, Jan. 2008.
- [34] J. Touboul, F. Wendling, P. Chauvel, and O. Faugeras. Neural mass activity, bifurcations, and epilepsy. *Neural computation*, 23(12):3232–3286, Dec. 2011.
- [35] A. Van Rotterdam, F. H. Lopes da Silva, J. van den Ende, M. Viergever, and A. Hermans. A model of the spatial-temporal characteristics of the alpha rhythm. *Bulletin of mathematical biology*, 44(2):283–305, 1982.
- [36] V. Volman, M. Bazhenov, and T. J. Sejnowski. Computational models of neuron-astrocyte interaction in epilepsy. *Frontiers in Computational Neuroscience*, 6:58, 2012.
- [37] V. Volman, E. Ben-Jacob, and H. Levine. The astrocyte as a gatekeeper of synaptic information transfer. *Neural Computation*, 19(2):303–326, Feb. 2007.
- [38] D. Wang and A. Bordey. The astrocyte odyssey. *Progress in neurobiology*, 86(4):342–367, 2008.
- [39] J.-M. Zhang, H.-K. Wang, C.-Q. Ye, W. Ge, Y. Chen, Z.-L. Jiang, C.-P. Wu, M.-M. Poo, and S. Duan. ATP released by astrocytes mediates glutamatergic activity-dependent heterosynaptic suppression. *Neuron*, 40(5):971–982, Dec. 2003.